BIOCYBERNETICS AND BIOMEDICAL ENGINEERING 43 (2023) 551—567

Available at www.sciencedirect.com

ScienceDirect

journal homepage: www.elsevier.com/locate/bbe

Original Research Article

Non-invasive waveform analysis for emergency triage via simulated hemorrhage: An experimental study using novel dynamic lower body negative pressure model

Naimahmed Nesaragi [a,*], *Lars Øivind Høiseth* [b], *Hemin Ali Qadir* [a], *Leiv Arne Rosseland* [b,c,d], *Per Steinar Halvorsen* [a,c], *Ilangko Balasingham* [a,e]

[a] *The Intervention Centre, Oslo University Hospital, Rikshospitalet, Oslo, Norway*
[b] *Division of Emergencies and Critical Care, Department of Anesthesiology, Oslo University Hospital, Oslo, Norway*
[c] *Institute of Clinical Medicine, Faculty of Medicine, University of Oslo, Oslo, Norway*
[d] *Department of Research and Development, Division of Emergencies and Critical Care, Oslo University Hospital, Oslo, Norway*
[e] *Department of Electronic Systems, Norwegian University of Science and Technology Trondheim, Trondheim, Norway*

ARTICLE INFO

Article history:
Received 30 November 2022
Received in revised form
5 June 2023
Accepted 14 June 2023
Available online 22 June 2023

Keywords:
Lower body negative pressure
Blood loss
Photoplethysmography
Noninvasive arterial waveform analysis
Deep learning
Time–frequency analysis

ABSTRACT

The extent to which advanced waveform analysis of non-invasive physiological signals can diagnose levels of hypovolemia remains insufficiently explored. The present study explores the discriminative ability of a deep learning (DL) framework to classify levels of ongoing hypovolemia, simulated via novel dynamic lower body negative pressure (LBNP) model among healthy volunteers. We used a dynamic LBNP protocol as opposed to the traditional model, where LBNP is applied in a predictable step-wise, progressively descending manner. This dynamic LBNP version assists in circumventing the problem posed in terms of time dependency, as in real-life pre-hospital settings intravascular blood volume may fluctuate due to volume resuscitation. A supervised DL-based framework for ternary classification was realized by segmenting the underlying noninvasive signal and labeling segments with corresponding LBNP target levels. The proposed DL model with two inputs was trained with respective time–frequency representations extracted on waveform segments to classify each of them into blood volume loss: Class 1 (mild); Class 2 (moderate); or Class 3 (severe). At the outset, the latent space derived at the end of the DL model via late fusion among both inputs assists in enhanced classification performance. When evaluated in a 3-fold cross-validation setup with stratified subjects, the experimental findings demonstrated PPG to be a potential surrogate for variations in blood volume with average classification performance, AUROC: 0.8861, AUPRC: 0.8141, $F1$-score:72.16%, Sensitivity:79.06%, and Specificity:89.21%. Our proposed DL algorithm on PPG signal demonstrates the possibility

* Corresponding author at: The Intervention Centre, Oslo University Hospital, Rikshospitelet Sognsvannsveien 20, 0372 Oslo, Norway.
E-mail address: naimahmed.nesaragi@gmail.com (N. Nesaragi).
https://doi.org/10.1016/j.bbe.2023.06.002

to capture the complex interplay in physiological responses related to both bleeding and fluid resuscitation using this challenging LBNP setup.

1. Introduction

Hemorrhage with blood volume loss is one of the leading potentially preventable causes of death in trauma patients [1]. Hypotension is a late sign during blood volume loss due to associated physiological compensatory mechanisms. For this reason, early diagnosis of ongoing mild to moderate hemorrhage is difficult, especially in young and healthy subjects. Even invasive arterial blood pressure (ABP), exhibits poor sensitivity due to human compensatory responses [2]. The other vital signs, including heart rate and blood oxygen saturation, also have low specificity and sensitivity for estimating blood volume loss.

Researchers have resorted to exploring various models that can artificially simulate hemorrhage. One such model is LBNP [3–5]. In this model of hypovolemia, healthy volunteers are placed in an air-tight chamber to which different levels of negative pressure is applied. This retains blood in the veins of the lower extremities and pelvis, creating graded central hypovolemia. Different LBNP-levels correspond to different levels of hypovolemia. Most studies to date [4–6], have applied LBNP in a predictable stepwise, progressive descending manner based on the hypothesis that *"as the time elapses there is a substantial steady and linear loss of blood among the test subjects"*. When testing algorithms for classifying levels of LBNP and degree of hypovolemia, this predictability based on time of LBNP can pose a problem. For instance, in a real-life pre-hospital emergency setting, volume resuscitation may be administrated during ongoing bleeding. We therefore propose an experimental setup with added degree of randomness in LBNP levels to avoid complete predictability by time. For the same reason, we also introduce unequal duration at each LBNP level. Hence, our proposed experimental setup is an attempt to emulate the patient with bleeding and fluid resuscitation as may be the case in pre-hospital treatment. This experimental model is more robust in the classification of the entire dynamic LBNP trajectory for the simulated hemorrhage. To our knowledge, no such reliable artificial intelligence method currently exists to predict the different likelihoods among the entire trajectory of applied LBNP, and thus assist to infer the stage of hemodynamic instability independent of time.

Recently, studies on artificial intelligence (AI) based algorithms have indicated that continuous analyses of noninvasive arterial waveform analysis (AWFA) reflect the information pertaining to the compensatory mechanisms compared to other standard vital signs [3,7,8]. Thus, making the earlier diagnosis of hemorrhage possible by the detection of hypovolemia prior to overt hemodynamic decompensation [9,10]. Hence, the design of such AI-driven predictive algorithms holds the potential to reduce morbidity and mortality among patients with hemorrhage [11,12]. In the initial screening of trauma patients, assessment is often restricted to the electrocardiogram (ECG), non-invasive photoplethysmography (PPG; giving arterial oxygen saturation), and blood pressure. The former two are routinely represented by continuous waveforms, whereas blood pressure is routinely measured intermittently in this clinical setting. Moreover, it is also possible to measure blood pressure continuously, either invasively or non-invasively [13,14], in an emergency setting. However, the PPG signal is generally considered a potential measure for variations in blood volume because of its ability to detect intravascular volume changes [1,2,15]. Prior studies have reported that PPG-based amplitude-derived features have the potential to measure dynamic blood volume loss [16]. Pulse-arrival-time [17,18] (based on both ECG and PPG) also known as pulse transit time is used in arterial wave propagation theory for blood loss estimation [19]. Current early hemorrhage detection studies based on machine learning (ML) approaches rely on AWFA that mostly employs morphological changes in the features of PPG signals [2,4,20–22]. However AWFA coupled with ML techniques and the aforementioned techniques involves complex feature extraction to capture the subtle information for the compensatory mechanisms in the arterial waveforms. Following are the limitations involved in the cumbersome feature extraction for PPG morphological theory and artery wave propagation theory: (i) In artery wave propagation theory, the fiducial points of each heartbeat in both ECG and PPG need to be extracted correctly [23,24]. (ii) This further adds the need to have proper sync among the two modalities and also both signals have to be of high quality. (iii) It is inevitable to have optimal filtering [25]. Hence, the morphological features are quite sensitive to signal quality, movement (placement) of the sensors, towards skin properties, and hence hinder the performance [26].

Unlike the analysis of non-invasive signals in the time-domain, which involves beat-to-beat quantification within a sole respiratory cycle, a sequence of breaths (5–10 typically) is quantified in the spectral analysis [15,27] for estimating blood volume loss. Prior studies [6,15] that coupled LBNP experiment setup with AI have efficiently used time–frequency (T-F) spectral methods for the assessment of blood volume loss in awake, spontaneously breathing subjects. The present study also focuses on the assessment of two non-invasive signals viz., ECG and PPG using high- resolution transient signatures based on T-F spectral analysis to detect progressive hypovolemia in awake spontaneously breathing subjects.

The present study aimed to (i) determine to what extent non-invasive ECG and PPG waveforms when coupled with ML (more specifically DL) predictive analytics can classify the degree of hypovolemia in healthy volunteers undergoing

LBNP with added randomness both in level and duration of each LBNP-level to reduce the effect of time, (ii) to compare the diagnostic capability of efficient T-F representation schemes with classical feature extraction methods.

2. Background and applications of LBNP

LBNP is a widely used technique to induce central hypovolemia, which triggers compensatory hemodynamic responses in humans [28]. Central hypovolemia triggers complex systemic compensatory responses, and understanding these responses is crucial. LBNP has been extensively employed to investigate the integrated physiological responses that occur during orthostasis, different levels of hemorrhages, and space-flight. Moreover, research on LBNP has been utilized to investigate seasonal variations in hormonal, autonomic, and circulatory states that affect LBNP-induced hemodynamic responses and tolerance, as well as sex-based differences during central hypovolemia and adaptations to exercise training [29–33]. The data generated from LBNP studies have contributed to the development of better models for predicting orthostatic tolerance [34], vasoconstriction [35], alterations in skin microcirculation dynamics [36], and countermeasures [37] against the effects of central hypovolemia.

Akin et al. [38] studied the acute effects of postural changes and the application of both lower body positive and negative pressures on the eyes. The effects of hydrostatic gradients and fluid shifts on the eye were investigated by inducing a fluid shift in both the supine and prone postures produced by LBNP and lower body positive pressure (LBPP). A similar study by Gallardo et al. [39] aimed to evaluate the changes that occur in parameters relating to muscle work and muscle hemodynamics under the influence of upright LBNP application during walking. The application of LBNP showed elevated work characteristics, mainly on the work output and less local muscle hemodynamics. The study hypothesized that LBNP-based treadmill could be a time-efficient training tool for stressing the musculoskeletal system, faster improve body composition and potentially enhancing cardio-respiratory fitness in general adult population. Kenny et al. explored the employment of LBNP protocol to develop a wireless ultrasound patch that can detect mild-to-moderate central hypovolemia. In these studies [40–42] a wireless, wearable Doppler ultrasound system that continuously measures the common carotid artery Doppler pulse was developed. A novel measure from this device, the Doppler shock index, accurately detected moderate-to-severe central blood volume loss in a human hemorrhage model generated by lower body negative pressure. A similar study by Raj et al. [43] investigated the ability of high-frame-rate ultrasound for calibration-free cuff-less carotid pressure system to capture dynamic responses of carotid pressure to LBNP and compared against the responses of peripheral pressure measured using a continuous BP monitor. A review study by Kimball et al. [44] explores the application of LBNP-induced hypovolemia and its association with health and performance problems common to occupational, military, and sports medicine using wearable sensors and machine learning. This review highlights and discusses the biological rationale for compensatory reserve and decompensation status and presents their sensitivity to numerous hypovolemia perturbations in human and animal models.

In the animal-based clinical study, by Berboth et al. [45] the researchers investigated the impact of incremental levels of LBNP on hemodynamic regulation in closed-chest pigs using invasive pressure–volume assessment. They found that as the preload was gradually reduced through LBNP, it caused negative pressures in the left ventricle of the heart, leading to increased suction and a more forceful pumping of blood. This increase in suction during relaxation, known as diastolic suction, is associated with central hypovolemia induced by LBNP. This study sheds light on the complex cardiovascular responses to LBNP-induced hypovolemia and could have implications for developing new treatments for related clinical conditions. A comparative study [46] between two different LBNP protocols, one using a continuous ramp protocol and the other using a traditional step protocol was carried out to compare tolerance and hemodynamic responses between these two LBNP profiles. The researchers found that the tolerance to lower body negative pressure (LBNP) induced by a continuous ramp protocol applied at a rate of 3 mmHg/min was similar to that of a traditional step protocol which progressively decreases in 5-min steps. Despite similar levels of central hypovolemia and hemodynamic responses between the ramp and step protocols, there were differences in the responses of cerebral blood velocity and oxygenation. The step protocol resulted in a greater increase in cerebral oxygen extraction and similar LBNP tolerance, likely due to facilitating the matching of metabolic supply and demand. The study highlights the importance of considering the pressure profiles when comparing LBNP-induced cardiovascular responses across different laboratories. Further research is needed to compare these responses to actual hemorrhage.

3. Materials and methods

3.1. *Study population and data sources*

The study was approved by the regional ethics committee (REK sør-øst C/ 2019/ 649). After written informed consent, 23 healthy volunteers aged between 18 and 40 years were included in the study. Pregnancy and/or cardiovascular disease with medication were exclusion criteria. Demographic information for the given study population is summarized in Table 1. Relevant information is presented as mean ± standard deviation, where applicable.

Table 1 – Study population demographics.

Factor	Subject Group (All Subjects)
Gender	(n = 23) 13 Female, 10 Male
Age	29.56 ± 3.55
Weight	71.15 ± 13.06
Height	173.39 ± 10.32
Body Mass Index	23.43 ± 2.77

Three-lead ECG was sampled from the Solar 8000i (GE Medical Systems) and a BioAmp/ PowerLab (ADInstruments, Bella Vista, Australia). PPG was sampled from a Masimo Radical 7 pulse oximeter, software 7.3.1.1 (Masimo Corp., Irvine, CA, USA). The sampling rate was 1000 Hz.

3.2. *Experimental protocol*

The experimental setup used a dynamic LBNP version to study hypovolemia as opposed to the traditional model, where LBNP is applied in a predictable step-wise, progressively descending manner. Fig. 1. shows the difference between the traditional and dynamic LBNP protocols. We refer the readers to [28] for preliminaries and further details on traditional LBNP setup. The lower part of the volunteers' body is subjected to a negative atmospheric pressure applied via the pressure chamber at the level of iliac crest as shown in Fig. 2. Blood is drawn towards legs and pelvis, to reduce central blood volume and thus emulate hemorrhage. Before the experiment started, the subject was familiarized with the setup resting in the supine position. Thereafter, the subjects were exposed to stepwise LBNP starting at 0 mmHg with unequal and abrupt changes in negative pressure, for every two or three minutes. To avoid complete predictability by time, a degree of randomness was added through the experiment as compared to the general trend of progressive descending LNBP as shown in Fig. 1. It is to be noted that in order to increase the total trials in this cohort study, each subject was subjected thrice to different dynamic LBNP experimental protocol. So, the resulting study cohort had 69 LBNP trials from 23 subjects. In the case of each subject, the experiment ended at the point of hemodynamic decompensation, indicated as a sudden decrease in arterial pressure and/ or symptoms of impending circulatory collapse such as loss of color vision (gray-out), nausea or dizziness bradycardia, or sweating [47]. Once the decompensation point was reached, the application of LBNP was released immediately to ambient pressure.

3.3. *ML framework for classification*

Fig. 3. shows the overview of the proposed DL-based predictive model development at the higher level with the key phases involved in the algorithm. The proposed DL-based framework is applied for both the non-invasive signals; ECG and PPG. However, for illustration only PPG signal is considered thought the article.

Fig. 2 – Illustration showing the test subject inside the lower body negative pressure (LBNP) chamber sealed just above the iliac crest.

3.3.1. *Data curation*

The complete trajectory of the LBNP trial comprises a baseline test followed by the onset of LBNP till the pre-syncope (i.e., end-stage of LBNP) as shown in Fig. 4 (a) or completion of the protocol. The various time points defining the hemodynamic decomposition levels in the entire trajectory of the LBNP trial are marked by employing the '*findchangepts*' function in MATLAB. The '*findchangepts*' function is based on parametric global method as described in studies [48] for signal changepoint detection. Hence this function can detect the abrupt changes in the LBNP trial accurately in terms of decomposition target levels as in Fig. 4 (b), thus establishing the ground truth. The mapping algorithm mentioned in Table 2 is then used to formulate the ground truth for the ternary classification among LBNP target levels. In order to

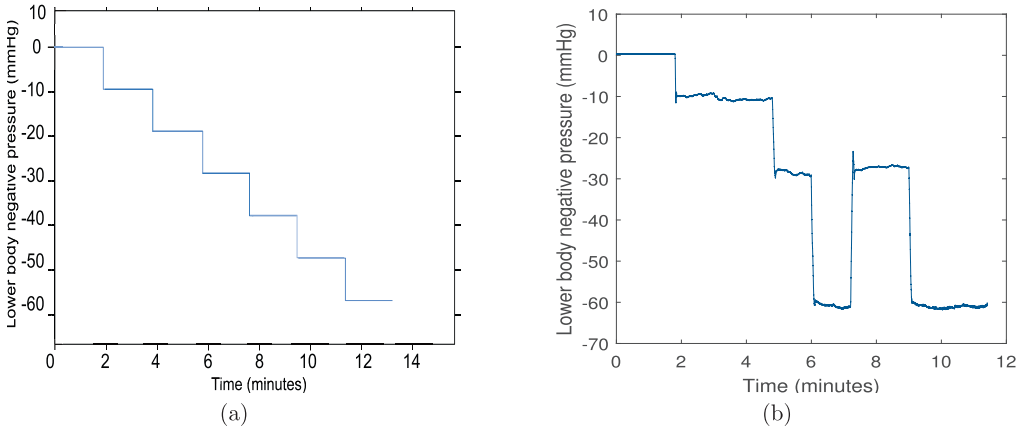

Fig. 1 – Illustration showing the difference between the progressive descending stepwise negative LBNP setup (a) and random LBNP experimental protocol as used in the present study (b).

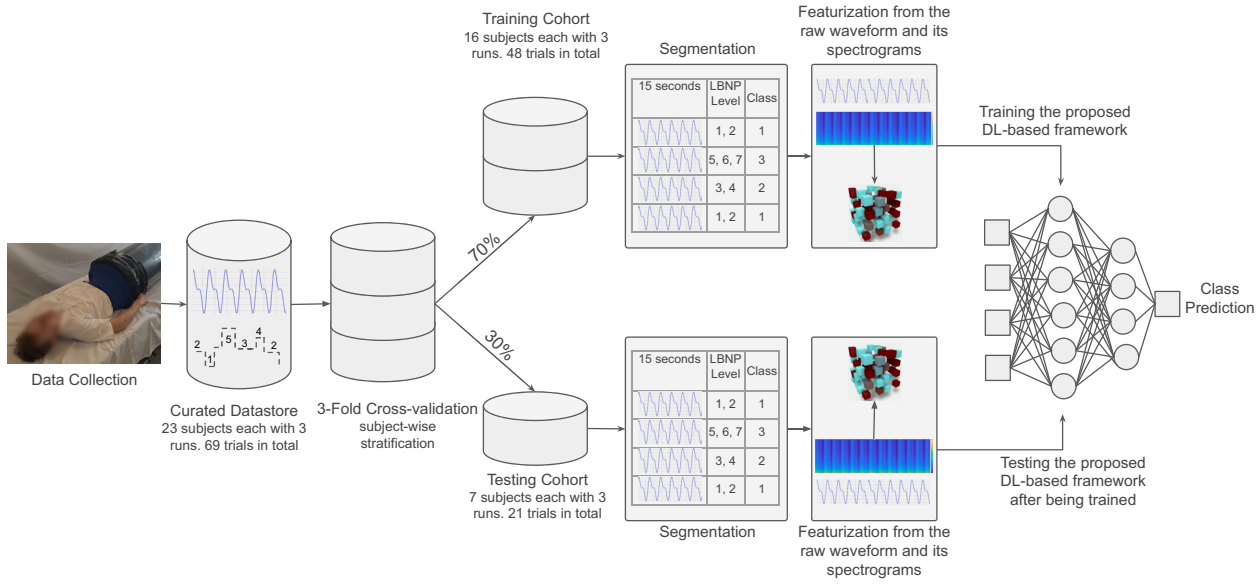

Fig. 3 – Phases of the proposed deep learning-based framework. The framework includes three main phases: i)*Data curation*, ii) *Featurization* of non-invasive pulse waveforms (both, ECG and PPG), and iii) *Model development* for classification. Data curation involves signal preprocessing, defining training and test cohorts based on subject stratification, segmentation of both cohorts, and annotation of waveform segments. Annotation is done by assigning different hemodynamic LBNP target levels and mapping them into three classes. Next, feature extraction is performed on raw waveform segments, and finally, a

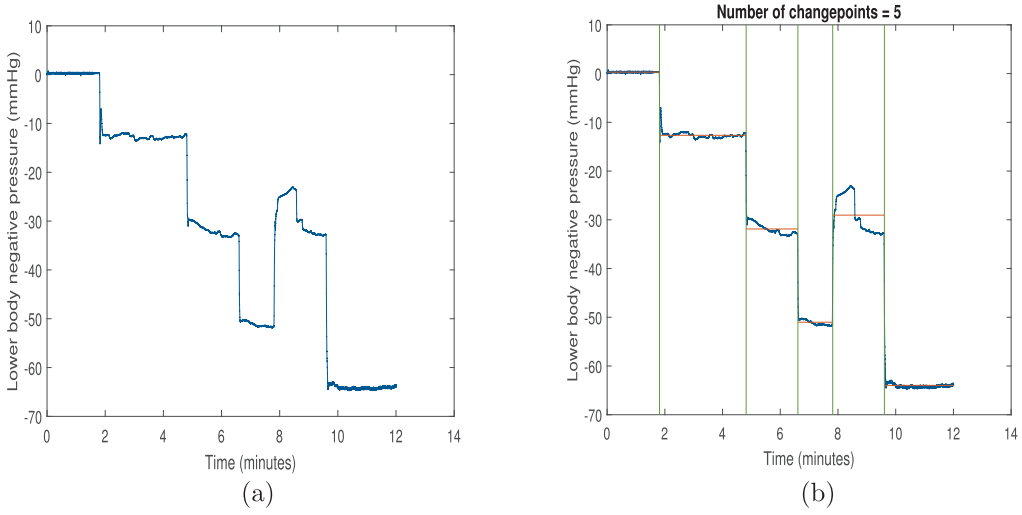

Fig. 4 – (a) Illustrates LBNP trial with N = 5 change points; (b) shows the detection of endpoints marked in time using the *'findchangepts'* function.

predict blood volume loss via LBNP trial, it is divided into 3 classes (Class 1 (mild):baseline to −10 mmHg; Class 2 (moderate): −20 to −30 mmHg; Class 3 (severe): over −40 mmHg). These levels correspond to estimated blood losses of 300–500 cc, 500–800 cc and greater than 800 cc respectively. This idea of association mapping between LBNP volume status to 3 classes for artificial distinction is inspired from the study performed by Soo-Yeon Ji et al. [49].

The *'findchangepts'* function takes the number of change-points *N* as input and accurately marks the end-points in time for each LBNP target level. Once the endpoints are detected, proper labeling of each time point with a target LBNP level for supervised machine learning becomes feasible. The abrupt changes in the LBNP trajectory trial are then modeled as a sequence of linear steps corresponding to the applied LBNP reference signal. As an illustration, linear and step-wise training targets for a particular LBNP trial are marked in Fig. 5 (a)-(c), together with the corresponding applied reference LBNP signal.

Once the ground truth is established a supervised DL-based framework is formulated to predict and classify the complete trajectory run of the LBNP reference signal. This is

Table 2 – The mapping algorithm to formulate the ground truth for the LBNP target levels.

Target Level	LBNP	Class Definition
1	0 mmHg	Class 1
2	−10 mmHg	
3	−20 mmHg	Class 2
4	−30 mmHg	
5	−40 mmHg	
6	−50 mmHg	Class 3
7	< −60 mmHg	

achieved by segmenting the underlying non-invasive waveform of each subject into equal segment lengths of 15 s with an overlap of 10 s. Physiologically, a segment length of 15 s duration is chosen so that it captures several (12–15) heartbeats comprising at least one respiratory cycle [3,47]. Each such waveform segment is associated with one of the three class definitions as ground truth defined in Table 2, and is treated as an individual sample of observation for training the proposed model. This results in a large number of observations as training samples from the original subjects with a limited number.

Next, feature extraction is performed on these waveform segments using time–frequency analysis on both non-invasive signals. The ML models are then trained with the derived feature set to classify each of 15 s waveform segments into either of the three classes.

3.3.2. *Classification model*

A unified DL-based model with multiple (two) inputs/branches is designed for the desired ternary classification task. The structure details with various layers in the respective branches of the proposed network architecture for the unified model is presented in Fig. 6. The designed unified model is constructed by training a mixture of two unique T-F representations for the respective branches, viz., T-F moments being fed to the upper input (Branch 1) of the network architecture as shown in Fig. 6. The detailed explanation of the feature extraction in terms of T-F moments derived from the spectrograms of given waveform segments is presented in the subsequent *section* 3.3.3. The lower input (Branch 2) of the network is initially fed with a raw waveform segment which is further converted into a logaritham scale-based 2-D spectrogram by custom-defined *'log spectrum layer'* to train the subsequent 2D-CNN layers. The need and advantage of such custom-defined *'log spectrum layer'* are also described in *section* 3.3.3.

3.3.3. *Featurization*

In this work, efficient feature extraction is realized by exploring T-F analysis of the underlying non-invasive signal. Thus the time-series signal in the 1-D domain as depicted in Fig. 7(a) is converted into the 2-D real plane (see Fig. 7(b)) to extract transient signatures. In literature, spectrogram-based T-F analysis, has been extensively employed with recurrent and convolutional neural networks (CNNs) to extract diagnostic signatures for various clinical applications [50,51]. However, dimensional reduction of the resultant time–frequency feature space can reduce the complexity of the algorithm and improve the classification performance with increased intelligibility for decision-making. This can be realised in practice by extracting T-F moments from the spectrograms. The present study explores two such moments in the T-F domain viz., spectral entropy (SE) and instantaneous frequency (IF) [50,52]. Figs. 7(c) and 7(d) illustrates the differences between IF and SE for windowed hemodynamic LBNP regions of the typical PPG signal. These T-F moments derived from the spectrograms of the noninvasive signal provide the best granular information of the two worlds, both fine-granularity and coarse-granularity. This can be explained as follows. For fine-granularity, first the given raw waveform segment of 15 s, sampled at 1000 Hz (corresponds to 15000 discrete time series) is first converted to length N of radix-2. i.e. $N = 2^n$, where n is a positive integer. This is achieved either by truncating the discrete time series or by padding it with zeros so that $N = 2^n$. In our case, for a discrete time-series with an initial length of 15000, the next close radix-2 number is

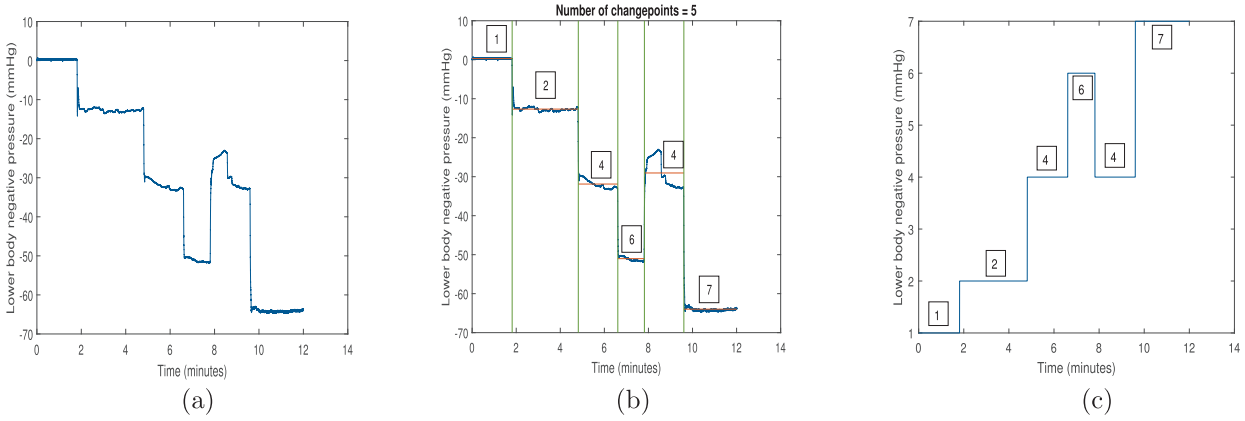

Fig. 5 – (a) Illustration of the applied reference LBNP trajectory signal inherited with abrupt changes(N = 5) among hemodynamic decomposition levels; (b) sequence of linear steps in "red" represents the profile of ground truth detected by the algorithm; (c) detected sequence of linear steps corresponding to the applied abrupt LBNP reference signal, later used as ground truth.

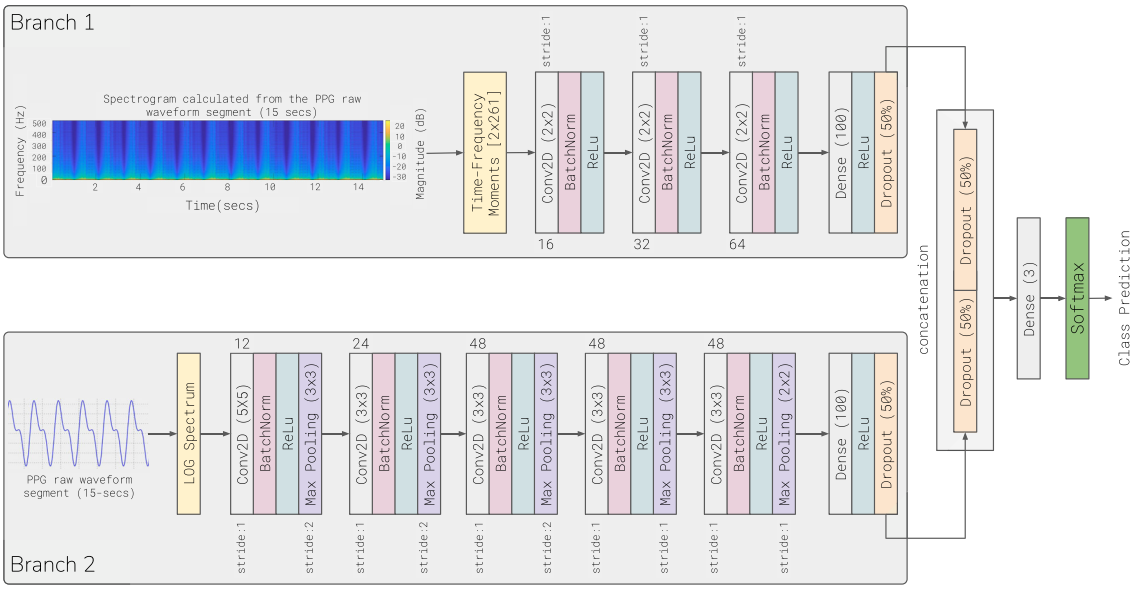

Fig. 6 – Network architecture of the proposed unified DL-based framework.

$N = 2^{14}$=16384. So the time-series segment is padded with zeros to increase its length to 16384. Then for finer-granularity the time series is binned with a window function of length 64 to form 256 time windows. Later, for coarse granularity, the central moment from power-spectrogram is computed, which corresponds to the center of the time windows.

The IF is the time-dependent frequency of a signal under interest and is computed as the first moment from the power spectrum that represents the spectral density resulting from short-time Fourier transforms as defined in Eq. (1), where $P(t,f)$ is the power spectrum of the time-window [53].

$$IF(t) = \frac{\int_{-\infty}^{\infty} fP(t,f)df}{\int_{-\infty}^{\infty} P(t,f)df} \tag{1}$$

For a given non-invasive signal (sampled at 1000 Hz) wave-form segment with a duration of 15 s, a feature vector of 256 lengths is obtained by computing spectrograms over 256-time windows. The output values are IF, in time, i.e. *IF (t)*, corresponds to the center of the time windows.

The SE combines the knowledge of spectrogram-based spectral density analysis with the information-theoretic measure- Shannon entropy [53]. SE reflects the degree of randomness (uncertainty) or the regularity (deterministic patterns) in the signal of interest. A spiky or random signal has low SE, while deterministic signals like white noise with a flat spectrum have higher SE values. The estimation procedure of SE is similar to IF and uses 256-time windows for the corresponding non-invasive signal waveform segment with duration of 15 s. However, SE considers the normalized power distribution in the frequency domain as a probability distribution of the signal and calculates its Shannon entropy. Therefore, the calculated Shannon entropy is contextually known as the SE of the signal. Given a T-F power spectrogram *P(t, f)*, the probability distribution at frequency point *n*, $n = 1,\ldots, N$; and time t, $0 \leqslant t \leqslant T$; denoted as *p(t, n)*, is:

$$p(t,n) = \frac{P(t,n)}{\sum_{f} P(t,f)}, \tag{2}$$

where $f \in [0, f_s/2]$, and f_s = 1000 Hz, sampling frequency. Then SE at time t, denoted as S(t), is given as [53]:

$$S(t) = -\sum_{n=1}^{N} p(t,n)\log_2 p(t,n). \tag{3}$$

The custom definition of '*log spectrum layer*' layer uses the '*dlstft*' function in MATLAB for computing short-time Fourier transforms that inherently support automatic backpropagation. The need and the advantage of such a custom realization of the network layer can be explained as follows. When any pre-processing steps, involving signal processing are performed outside the DL network, then predictions might differ due to different pre-processing settings in comparison to those used in training of the network [54]. This can impact the performance of the network (to be poorer than expected). Placing the pre-processing computations (in this case spectrograms) inside the network as a layer results in self-contained model and simplifies the pipeline for deployment with efficient handling of storage. The logarithm-based scale of the spectrogram is considered in training the deep networks because it acts like a dynamic range compressor. This boosts the representation scheme having values with small magnitudes (amplitudes) but still carrying important information.

4. Experiments and results

4.1. *Dataset stratification for cross-validation*

The proposed framework performed predictive analytics on the given non-invasive wave-form segments of both ECG and PPG signals from the patient records to determine the degree of risk in hypovolemia development by classifying the reference LBNP trajectory into 3 classes. The experimental

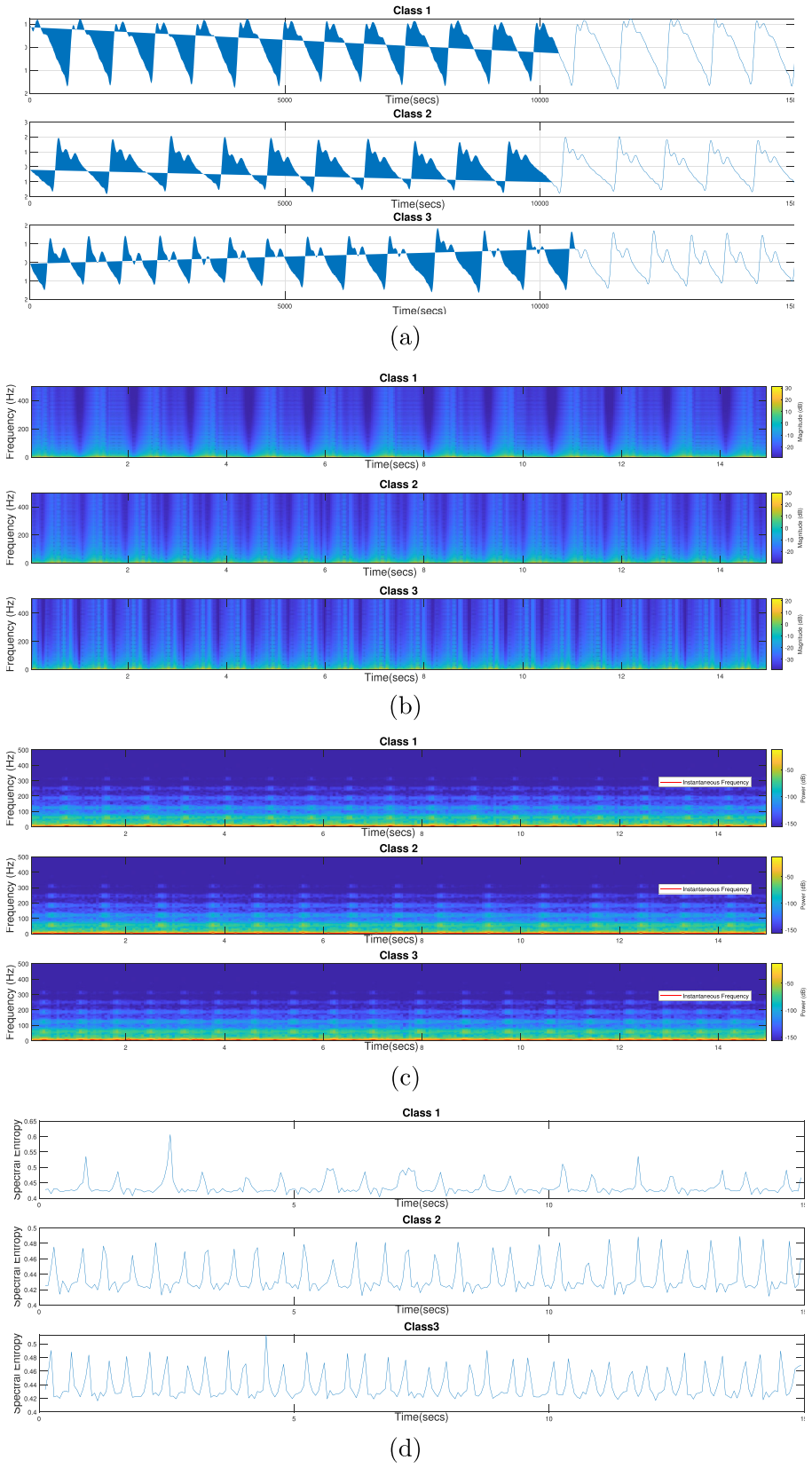

Fig. 7 – (a) Illustration of raw PPG waveform segments for the three different classes; (b) Spectrograms derived from the raw PPG waveform segments shown in (a); (c) Instantaneous frequencies; (d) Spectral entropies computed from the spectrograms shown in (b).

study was performed using threefold cross-validation based on a patient-wise stratification scheme, with each fold containing a unique ~30% of the entire dataset. i.e., The model is trained and developed using ~70% (16 subjects) of total data and the remaining ~30% (7 subjects) data is considered for validation. Thus, the total data comprising 23 subjects is divided into stratified, three unique training and test sets containing 16 and 7 subjects respectively to perform threefold cross-validation.

Defining stratified cohorts in terms of individual subjects is very much important during training and testing, since over-fitting (high variance) is usually observed in experiments where validation waveform segments are selected from the pool of all subjects. It is to be noted that each subject is subjected thrice to the LBNP experimental protocol. So, the resulting training cohort included training waveform segments with 48 LBNP trials from 16 unique subjects and the testing cohort included waveform segments with 21 LBNP trials from the remaining unique 7 subjects. The sample distribution of waveform segments in the threefold validation setup is listed in Table 3. Further it is worth mentioning that the overlap of 10 s duration is performed only during training and is omitted during the segmentation of test subjects, to keep the ratio of 3:1 among the waveform segments of train and test cohorts.

4.2. Model design and training

The proposed DL-based classification model was developed using the DL toolbox in MATLAB with NVIDIA GeFore GTX 1080Ti. In a 3-fold cross-validation setup, the proposed model was trained on subject-wise stratified three-folds and the optimized hyper-parameters that minimize the cross-validation loss are listed in Table 4. The optimal network hyper-parameters and training options were obtained by performing Bayesian optimization using '*Experiment Manager*' in MATLAB. An objective function was formulated for the underlying Bayesian optimization on model hyper-parameters that intend to maximize the F1-score.

Table 3 – Sample distribution of waveform segments for model training and validation in 3-fold cross-validation.

	Training		
	Fold 1	Fold 2	Fold 3
Class 1	1263	1215	1174
Class 2	1843	1866	1955
Class 3	1997	2079	2055
Total	5103	5160	5184
	Testing		
	Fold 1	Fold 2	Fold 3
Class 1	301	333	365
Class 2	601	582	598
Class 3	633	582	546
Total	1535	1497	1509

Table 4 – Optimized model hyper-parameters with training option values.

Model hyper-parameters & Training options	Values
L2_Regularization	0.1
BatchSize	10
learning_rate	0.001
LearnRateDropFactor	0.1
LearnRateDropPeriod	20
LearnRateSchedule	*piecewise*
MaxEpochs	80
Optimizer	SGD

The model was trained using the stochastic gradient descent optimizer (SGD) with the help of the cross entropy loss given by:

$$L = -\sum_{i=1}^{n} t_i \times log(p_i), \tag{4}$$

where t_i is the true label and p_i is the softmax probability for the *ith* class and n is the number of classes.

4.3. Results of the proposed framework

Tables 5 and 6 present the classification performance of the proposed method in a 3-fold cross-validation setup for both non-invasive signals, ECG and PPG respectively. The experimental results are initially evaluated and verified using the area under the receiver operating characteristic (AUROC) curve analysis in one vs others format for multi-class scenario. As an illustration, the individual AUROCs for each class with their corresponding model operating point, together with the average AUROC value for each fold, in a 3-fold cross-validation setup for PPG signal is shown in Fig. 8. However, there exists a severe imbalance in data points among the three classes in terms of the available number of waveform segments. Hence, average precision-recall curves are also analyzed as shown in Fig. 9. Further, the harmonic mean between precision and recall, i.e., F1-score is also presented in Tables 5 and 6.

4.4. Ablation experiments

Further, to justify and emphasize the clinical performance of the proposed unified network architecture, a subjective analysis of the latent space derived from the late-fusion at the end of DL unified model is done against the ablation experiments. These ablation studies involve testing the performance of the individual model in a respective branch on the desired classification by excluding the computation of other branch model.

As a part of the aforementioned ablation experiments, we performed two well-tuned individual model training methods. In the first method, the model trained only with T-F moments from branch 1 of Fig. 6 is considered excluding the effect of '*log spectrum layer*' from branch 2 of the unified DL model. For the latter ablation method the experimental setup is vice versa. The results for these ablation experiments are also presented in Tables 5 and 6 for ECG and PPG signals respectively. Model hyper-parameters were always consistent

Table 5 – Summary of cross-validation results for the proposed method and the ablation experiments on ECG signal.

Models	T-F moments	Log-spectrograms	AUROC	$F1_{score}$	Sensitivity	Specificity
Branch 1	✓	✗	0.6732	53.12	61.14	69.05
Branch 2	✗	✓	0.6432	49.12	57.14	61.05
Proposed Study	✓	✓	**0.6953**	**56.67**	**59.45**	**69.77**

Table 6 – Summary of cross-validation results for the proposed method and the ablation experiments on PPG signal.

Models	T-F moments	Log-spectrograms	AUROC	$F1_{score}$	Sensitivity	Specificity
Branch 1	✓	✗	85.64	68.81	67.74	84.90
Branch 2	✗	✓	84.72	67.98	66.22	83.45
Proposed Study	✓	✓	**0.8861**	**72.16**	**79.06**	**89.21**

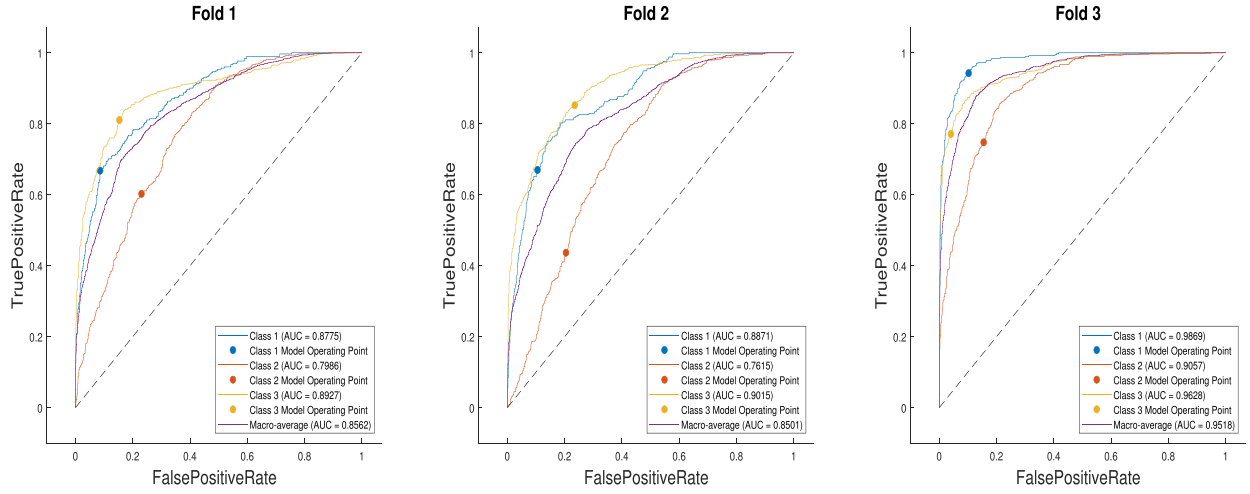

Fig. 8 – Receiver-operating characteristic curves displaying the ability of the proposed unified model to perform the desired classification task in a 3-fold cross-validation setup for PPG signal.

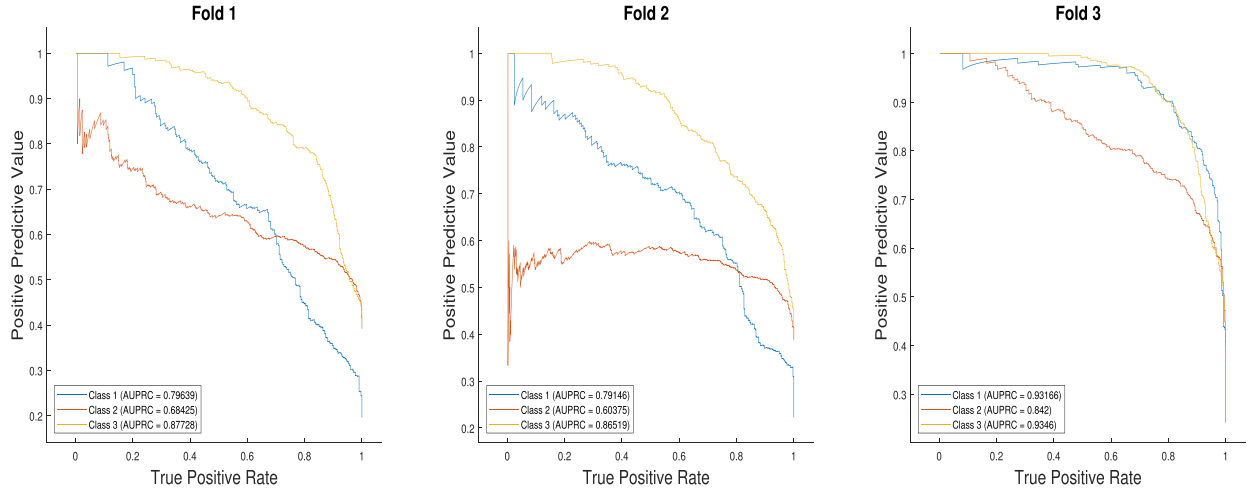

Fig. 9 – Precision-Recall curves displaying the ability of the proposed unified model to perform the desired classification task in a 3-fold cross-validation setup for PPG signal.

across these evaluations as enlisted in Table 3. As seen in Tables 5 and 6, the performance of the proposed unified model alone with late fusion was significantly higher in comparison to the individual ablations and further, the PPG signal outperformed ECG using the proposed unified model.

4.5. *Comparative experimental analysis*

The most commonly studied theories in the research context of artificial distinction within simulated hemorrhage are arterial waveform analysis, which explores features in terms of fiducial points obtained from PPG derivatives and the heart (pulse) rate variability i.e., HRV (PRV)-based features from ECG and (or) PPG. Further, PPG morphological theory is also studied that mainly explores PPG signals. As mentioned earlier in *section* 3.3.3 this study used raw waveform segments and explored time–frequency representations to capture the transient signatures for the desired classification task. The reason behind resorting to T-F representations was to eliminate the limitations (mentioned in the introduction) exhibited by the cumbersome feature extraction involved in classical methods of AWFA (PPG morphological theory, HRV, PRV and artery wave propagation theory).

To support our hypothesis that the proposed T-F-based DL approach on given waveform segments is more efficient than the above-mentioned classical methods, we perform the comparative analysis with the following baseline studies w. r.t. two noninvasive modalities i.e. ECG and PPG.

4.5.1. *ECG analysis*

- HRV features: Inter-beat-interval information is obtained by calculating the RR interval of each waveform segment. Pan-Tompkins algorithm is employed to efficiently detect QRS wave and subsequently the R peaks. HRV-based features in time and frequency-domain are extracted from the derived RR intervals [55]. More details on HRV based features are presented in Table A1 of Appendix A.

- Nonlinear features: Several nonlinear signatures from ECG were extracted. Entropy-based features inspired from the research Entropy-hub [56], auto-regressive coefficients from the model with order 4, Shannon entropy values from the sub-bands resulting using level 4 decomposition on maximal overlap discrete wavelet packet transform [57], and Multifractal wavelet-based features of the scaling exponents were also extracted. These nonlinear features were chosen as per the state-of-the-art research demonstrating their effectiveness in various ECG classification tasks. Detailed explanation of the extracted nonlinear features is presented in Appendix A.

- Time–frequency analysis: Various T-F representations viz., scalograms, spectrograms, and wavelet scattering etc., were also explored to capture the transients of the ECG signal waveform segments. However, the scalogram-based CNN-LSTM DL model yielded better performance among T-F analysis.

Table 7 – Summary of comparative analysis for the classification performance between the proposed method and baseline studies in 3-fold cross-validation setup.

Method used	(#) Features	Classifier	AUROC	$F1_{score}$	Sensitivity	Specificity
ECG analysis (HRV + nonlinear)	55	Bag Decision Trees	0.6432	49.12	57.14	62.05
ECG analysis Time–frequency	2D Scalograms	CNN-LSTM	0.7778	61.64	65.07	81.09
PPG analysis (Fiducial-points Morphological)	48	AdaBoost	0.7664	58.62	57.74	79.13
PPG analysis (PRV + nonlinear)	55	Bag Decision Trees	0.6928	55.67	59.92	69.72
Proposed Study (PPG)	**T-F moments + log-spectrograms**	**Unified DL Model**	**0.8861**	**72.16**	**79.06**	**89.21**

Table 8 – Summary of ML-based clinical studies performed using LBNP for automated detection of simulated hemorrhage and (or) classification of blood volume decompensation.

Research Study	Methods (Features)	Model	Results
Convertino et al. [4]	Non-invasive hemodymaic features: BP, $EtCO_2$, pulse character, and respiratory rate	Regression Analysis Leave-one-subject-out strategy	Accuracy: 96.50% Correlation Coefficient(R): 0.89
Convertino et al. [3] Techentin et al. [47]	CRI & CRM	Logistic Regression Analysis, CNN 10% hold out validation	Binary classification AUROC: 0.9268 (CRM) AUROC: 0.9164 (CRI)
Bjorn J.P.van der et al. [5]	BP Curve dynamics, SV, CO, $EtCO_2$, TCD	SVM Leave-one-subject-out strategy	3-class classification study Sensitivity: 78.21% Specificity: 91.51%
Bjorn J.P.van der et al. [60]	1-D Cubic Hermite splines interpolation + PCA	SVM Leave-one-subject-out strategy	4-class classification study Accuracy: 57% MSE: 0.26 Kappa: 0.4650
Soo-Yeon Ji et al. [6]	HRV analysis + Wavelet Transformation	LibSVM Leave-one-subject-out strategy	Binary classification Accuracy: 89.1% AUROC: 0.86 3-class classification study Accuracy: 69.5%
Fadil et al. [61]	Wavelet transform coherence + Causality analyses.	Logistic Regression Analysis Leave-one-subject-out strategy	Binary classification (LT vs HT) Accuracy: 63% - 89.1% AUROC: 0.74–0.86 Accuracy: 63% - 84% Sensitivity: 58% - 83% Specificity: 71% - 86%
Kugener et al. [62]	Modified ResNet50 using the ImageNet weights	Long short term memory Network	automated (image-only) RMSE of 358 mL (R^2 = 0.4) Accuracy: 85%. semiautomated (image + locations) RMSE of 260 mL (R^2 = 0.7) Accuracy: 90%.
Gupta et al. [63]	half-rise to dicrotic notch (HRDN) feature	Gradient-boosted regression trees	RMSE: 13% (R^2 = 0.4) AUROC: 0.97
Chalumuri et al. [65]	Fiducial points - derived from multiple physiological signals	Three ML classifiers considered (i) logistic regression, (ii) random forest, and (iii) support vector machine. Leave-one-subject-out strategy	Final multi-class classifier Accuracy: 81% - 90% *F1Macro*: 77 ± 11
Proposed Study	Time–Frequency Moments + Log Spectrograms	Unified DL Model 3-fold cross-validation	AUROC: 0.8861 AUPRC: 0.8141 $F1_{score}$: 72.16 Sensitivity: 79.06% Specificity: 89.21%

4.5.2. *PPG analysis*

- Fiducial points-based features: A comprehensive investigation in terms of morphological characteristics of the PPG signal and its derivatives was carried out according to the recommendation in the research [2,20]. The detection of the fiducial points assists in extracting time, amplitude, locations, and finally morphological area of the underlying signal. These signatures have been widely employed for tracking hemodynamics [58,59]. These investigated features are detailed in Table A2 of Appendix A.

- Pulse-rate variability (PRV) and Nonlinear features: Similar to ECG-based HRV analysis, PPG-based PRV features, and other nonlinear features were extracted.

Table 7 represents the comparative analysis of the classification performance between the proposed method and the baseline studies. Table 7 shows that the classification performance of PPG-based T-F representations with the proposed unified model outperformed ECG signal and also significantly higher than other baseline studies performed with classical methods for ECG and PPG. It is worth mentioning that the proposed unified framework with the same hyper-parameters enlisted in Table 4 with appropriate modifications in network architecture was applied on the underlying classical methods for ECG and PPG. However, the proposed model did not perform better compared to the respective classifiers listed in Table 7. This means only the results of the best performing classifiers are shown in Table 7.

5. Discussion

The ternary classification results obtained from the proposed study demonstrate the possibility for the design of ML models using non-invasive waveforms to classify the level of hypovolemia prior to overt hemodynamic decompensation in healthy volunteers undergoing LBNP. The unique transient signatures captured and learned by the proposed unified model from the raw waveform data are quite efficient compared to the classical morphological features. This is hypothesized by our comparative results of the classification performance between the proposed versus the classical feature extraction techniques.

ML techniques in comparison to statistical methods are data-driven and impart a comprehensive way toward reliable diagnosis and prognostication. Contemporary research studies on hemodynamic monitoring and its management strategies for the diagnosis of blood loss have been widely addressed by the development of such ML models. However, in retrospect, providing a straightforward and direct comparison among these ML-based studies on hemodynamic instability is a tedious task because of certain reasons. viz., In these studies, generally the context of each problem to be addressed is varied. Some of the studies demonstrated that, forecasting the trend of certain vital signs by the ML models, learned with the initial partial part, can herald the condition of hemodynamic instability. Few of other studies tried to translate the model outputs into categories of physiological events, merely to have an artificial distinction for the classification task. Even variability exists among the experimental setup in terms of signal acquisition. Further, for the validation different performance metrics are used.

Table 8 summarizes ML-based clinical studies employing LBNP for automated detection and classification of simulated hemorrhage. A research study [4] led by Convertino et al. developed a novel ML-based experimental setup using LBNP to estimate CBV loss with 96.5% accuracy. The correlation between actually applied LBNP levels and the prediction for hemodynamic decompensation using forecasting was 0.89. Non-invasive hemodynamic features were used in the design

of ML model that mainly includes vital signs during surgery viz., blood pressure, $EtCO_2$, pulse character, and respiratory rate. More specific to the topic of classification among physiological events under simulated hemorrhage via LBNP experimental settings, the same group by Convertino et al. performed a binary classification between Low versus High tolerance categories towards reductions in CBV [3]. A Logistic regression (LR) analysis by regressing the onset of decompensated shock was performed using two unique compensatory reserve algorithms viz., CRM (compensatory reserve metric) and CRI (compensatory reserve index). Further, the performance of LR analysis was compared against DL model (CRM-DL) using 1-D CNN with the estimated CRM values on the same LBNP datasets [47]. The performance yielded in terms of AUROCs to be 0.9268 (CRM) and 0.9164 (CRI) respectively. Recently, the same group reported a study led by Bedolla et al. [64] on the development of an explainable machine learning model for measuring compensatory reserve. Here the authors claimed to focus on feature extraction methodologies for tracking CRM using 10 waveform features as opposed to millions of tuned AI model parameters. Overall, model performance was similar to a more complex deep-learning model, and by tracking extracted features, differences were identified in subgroups in the data sets. Fadil et al. [61], explored the possibility of using the interaction between heart rate, blood pressure, and cardiorespiratory coupling to monitor the development of simulated hemorrhage through LBNP. This study also aimed to differentiate individuals with high tolerance (HT) to hypovolemia from those with low tolerance (LT). Bjorn J.P.van der et al. [5] developed a Support vector machine (SVM) - based predictive algorithm to perform ternary classification of impeding simulated hypovolemic shock using LBNP. The model features included, BP curve dynamics, volumetric hemodynamic parameters (both SV and CO), $EtCO_2$, and middle cerebral artery transcranial Doppler (TCD) blood flow velocity. The average sensitivity and specificity for the ternary classification using *'leave-one-subject-out'* validation were 78.21% and 91.51% respectively. Further, Bjorn J.P.van der et al. also reported results for a 4-class classification study [60] with accuracy, mean square error and Kappa score of 57%, 0.26, and 0.4650 respectively. HRV analysis using ECG was done by Soo-Yeon Ji et al. [6] by applying wavelet-based ML predictive algorithms for the prediction of induced central hypovolemia via LBNP as a surrogate of hemorrhage. The average accuracy and AUROC for binary classification were 89.1% and 0.86 respectively and for ternary classification accuracy of 69.5% is obtained using leave-one-subject-out validation. Kugener et al. [62] introduced a new DL system that accurately assesses blood loss (BL) and the success of hemorrhage control during endoscopic endonasal surgery using video from cadaveric training exercises. The proposed DL pipeline took input video as a sequence of images and predicts BL and task success using either only images (automated model) or images with human-labeled instrument annotations (semi-automated model). The performance of these models was compared against two reference models: one using average BL across all trials (control 1) and another using linear regression with time to hemostasis as input (control 2). The models were evaluated using RMSE and correlation coefficients, with a lower RMSE indicating better performance. Gupta et al. [63] reported a research study based on the novel data that simulates both whole blood hemorrhage and resuscitation at varying rates. This study claimed that half-rise to dicrotic notch (HRDN) feature, trained with a gradient boosting tree model, can detect blood loss and resuscitation with similar accuracy and performance as more complicated deep learning-based systems reported in other studies. Chalmuri et al. [65] developed a novel computational ML algorithm to estimate blood volume decompensation state based on analysis of multi-modal wearable-compatible physiological signals from swine subjects. The classification of blood volume decompensation state was limited not only to discriminate normovolemia from hypovolemia but also classify hypovolemia into absolute hypovolemia and relative hypovolemia. Leave-one-subject-out analysis on six animals achieved an average F1 score and accuracy of 0.93 and 0.89 in classifying normovolemia vs. hypovolemia, 0.88 and 0.89 in classifying hypovolemia into absolute hypovolemia and relative hypovolemia, and 0.77 and 0.81 in classifying the overall blood volume decompensation state.

All of the clinical studies existing to date, for the simulated hemorrhage deployed LBNP experimental setups based on negative pressure that progressively descends step-wise with equal duration at each level and thus make the event to be biased with time dependency, with the hypothesis that as time elapses, there is continuous bleeding.

The proposed dynamic LBNP protocol with added randomness in LBNP levels and duration of levels was to reduce the effect of time and to mimic a more relevant clinical scenario where a bleeding patient receives fluid resuscitation from health personnel at the site of the accident or in the ambulance on the way to the hospital. Fluid resuscitation changes central blood volume. Typically, it is done intermittently with various rates, volumes and times, depending on a subjective evaluation of both the amount of the bleeding and the effects of interventions to stop the bleeding. As a consequence, the fluctuations in central blood volume can be large and rapid as simulated in our model. The results of our study were based on ML analysis of routine non-invasive vital signs as used in an ambulance. ECG and PPG are the only continuous monitoring modalities in this setting. An important finding was that the PPG signal performed better than ECG in classifying levels of bleeding. This means that reliable monitoring of changes in central blood volume is possible by solely using a finger probe PPG during LBNP-induced hypovolemia. These findings are in line with recent studies [66–68]. The studies [67,68] focused specifically on PPG waveforms recorded during the LBNP experiment. The results of the study [68] reveal that analyzing the amplitude and phase dynamics of PPG waveforms during LBNP can provide valuable information about physiological changes. Specifically, the findings hypothesized that the phase difference between higher-order harmonics and fundamental components changes more significantly when the PPG signal is recorded from the ear compared to the finger at the beginning of the study. On the other hand, during the recovery period, the amplitude changes in the finger PPG are more prominent than in the ear PPG. Further, researchers in [67] explored the ear PPG waveform as an example of a central site during LBNP-induced hypovolemia. This study hypothesize

that the ear PPG waveform, particularly the phase hemodynamic index (PHI), provides information about progressing central hypovolemia, and has the potential to serve as an early predictor in such clinical settings. Overall, these findings suggest that a comprehensive harmonic analysis of PPG waveforms can offer new insights into hemodynamic changes during physiological challenges like LBNP. The differential behavior of phase and amplitude measurements between ear and finger recordings indicates distinct physiological responses and highlights the potential of using PPG waveform analysis for studying LBNP-induced hypovolemia.

PPG waveform contains information on heart rate, and pulsatile volume in addition to arterial oxygenation of the patient. Respiration, sympathetic nervous system activity, and thermoregulation also influence the waveform. Our proposed ML algorithm captured this complex interplay in physiological responses to different levels of bleeding. From a clinical point of view, in the case of bleeding and fluid resuscitation, a method should also provide reliable information on treatment effects in order to avoid serious complications related to fluid overload. Our proposed ML algorithm on PPG signal demonstrates this possibility in this challenging LBNP setup. The PPG signal is usually of high quality in comparison to ECG, even during movement of the patient. This makes it likely that the ML algorithm can provide accurate early recognition and analysis of bleeding.

Some of the limitations of our proposed study that need to be explored further in prospective real-time clinical deployment are as follows. Healthy subjects who were exposed to negative pressure via the experimental setup, mimic similar physiology of hemodynamics to that of subjects undergoing hemorrhage. However, they differ from the ones with actual bleeding because they were neither in pain, nor anxiety nor they had a disruption in actual tissues. Hence the complete translation of this experimental model to the actual scenario of patients in trauma with hemorrhage shock is not true. However, the proposed experimental setup imparts a peerless monitoring opportunity of vital physiological changes in real-time that can map the compensatory responses to progressive central hypovolemia similar to that caused by bleeding. Even, previous LBNP trials exhibited identical physiologic responses to those of actual volume loss during the early compensatory phases of hemorrhage.

Distribution of the waveform segments among the three classes highly varied as input observations to the model. The '*mild*' (Class 1) blood loss had a fewer observations. compared to '*moderate*' and '*severe*' blood loss classes. In case if the model was trained on relatively equal number of waveform segments among the three classes, then there could have been significant effect on the classification performance. However, the models trained with imbalanced data are still obliged to assign prediction labels to each waveform segment through the whole LBNP trajectory from normal- to hypovolemia among the three classes. This reflects in the output with the overall high specificity, since the miss-classification of an observation w.r.t., investigated class could result in observation belonging to either of the two remaining classes.

There is no straightforward linkage in mapping the physiological events comprising of given LBNP trajectory, translating to the output of the DL-based AI model. i.e., three class definitions from normal- to hypovolemia, were created merely to accomplish an artificial distinction among the ongoing hemodynamic decompensation towards progressive central hypovolemia. From a clinical perspective, it is still debatable to comment that the underlying physiological responsive events may fit (or) not fit into these classes, and hence classification performances thus reported may not reflect the direct classification of underlying physiology. However, changing probabilities by the DL model among the class definitions quantify model performance that hints at the progression of hemodynamic instability respectively.

6. Conclusion and future work

This study aimed to investigate the potential of advanced waveform analysis and deep learning algorithms in diagnosing levels of hypovolemia using non-invasive physiological signals. A modified dynamic LBNP experimental protocol is used to circumvent the problem posed in terms of time dependency, as in real-life pre-hospital settings intravascular blood volume may fluctuate due to volume resuscitation. The results demonstrated that a supervised deep learning-based framework, trained on raw PPG waveform segments and their time–frequency representations, accurately classified each segment into blood volume loss categories. These findings highlight the potential of PPG as a surrogate for blood volume variations and the effectiveness of time–frequency spectral methods in assessing blood volume loss.

Future efforts will focus on evaluating the discriminative ability of machine learning models using a diverse collection of data encompassing different human experimental protocol settings. The study acknowledges the limitation of the cohorts being limited to healthy volunteers and emphasizes the need for experimental protocols involving patients with various medical conditions to enhance the model's diagnostic capabilities. While a cross-validation approach was used to evaluate the proposed method's performance, further testing on a larger and more diverse dataset is necessary to fully assess its efficacy, generalizability, and safety. Additionally, the study plans to explore the application of time-series transformers on non-invasive waveforms to eliminate the need for feature extraction and enhance the model's performance using a multi-head attention mechanism.

Funding

This work was supported in part by the Health South East Authority in Norway, Helse Sør-Øst RHF (HSØ: New Real-time Decision Support during Blood Loss using Machine Learning on Vital Signs) under Grant No. 19/00264–202, and Prosjektnummer 2020079.

Ethical Approval

The study was approved by the regional ethics committee (REK sør-øst C/ 2019/ 649). After written informed consent, 23 healthy volunteers aged between 18 and 40 years were included in the study. Pregnancy and/or cardiovascular disease with medication were exclusion criteria.

CRediT authorship contribution statement

Naimahmed Nesaragi: Conceptualization, Formal analysis, Methodology, Software, Validation, Writing – original draft. **Lars Øivind Høiseth:** Conceptualization, Data curation, Writing – review & editing. **Hemin Ali Qadir:** Conceptualization, Writing – review & editing. **Leiv Arne Rosseland:** Resources, Supervision, Writing – review & editing. **Per Steinar Halvorsen:** Funding acquisition, Investigation, Methodology, Project administration, Resources, Supervision, Writing – review & editing. **Ilangko Balasingham:** Project administration, Resources, Supervision.

Declaration of Competing Interest

The authors declare that they have no known competing financial interests or personal relationships that could have appeared to influence the work reported in this paper.

Acknowledgment

The authors acknowledge the support provided for the experimental setup by Jonny Hisdal, from Faculty of Medicine, University of Oslo, and Section of Vascular Investigations, Oslo University Hospital, Oslo, Norway. Consultant Marius Erichsen from Division of Emergencies and Critical Care, Department of Anesthesiology, Oslo University Hospital, for including volunteers and participating in the LBNP experiments. Consultant Sverre Nestaas from Division of Emergencies and Critical Care, Department of Anesthesiology, Oslo University Hospital, for participating in preparing the dataset for analysis.

Appendix A. Supplementary data

Supplementary data to this article can be found online at https://doi.org/10.1016/j.bbe.2023.06.002.

REFERENCES

[1] Convertino VA, Cardin S. Advanced medical monitoring for the battlefield: a review on clinical applicability of compensatory reserve measurements for early and accurate hemorrhage detection. J Trauma Acute Care Surg 2022;93(2S): S147–54.
[2] Chen Y, Hong C, Pinsky MR, Ma T, Clermont G. Estimating surgical blood loss volume using continuously monitored vital signs. Sensors 2020;20(22):6558.
[3] Convertino VA, Techentin RW, Poole RJ, Dacy AC, Carlson AN, Cardin S, et al. AI-enabled advanced development for assessing low circulating blood volume for emergency medical care: comparison of compensatory reserve machine-learning algorithms. Sensors 2022;22(7):2642.
[4] Convertino VA, Moulton SL, Grudic GZ, Rickards CA, Hinojosa-Laborde C, Gerhardt RT, et al. Use of advanced machine-learning techniques for noninvasive monitoring of hemorrhage. J Trauma Acute Care Surg 2011;71(1):S25–32.
[5] Van Der Ster BJ, Bennis FC, Delhaas T, Westerhof BE, Stok WJ, Van Lieshout JJ. Support vector machine based monitoring of cardio-cerebrovascular reserve during simulated hemorrhage. Front Physiol 2018;8:1057.
[6] Ji SY, Belle A, Ward KR, Ryan KL, Rickards CA, Convertino VA, et al. Heart rate variability analysis during central hypovolemia using wavelet transformation. J Clini Monitor Comput 2013;27(3):289–302.
[7] Chew MS, Đneman A. Haemodynamic monitoring using arterial waveform analysis. Curr Opin Critical Care 2013;19 (3):234–41.
[8] Convertino VA, Grudic G, Mulligan J, Moulton S. Estimation of individual-specific progression to impending cardiovascular instability using arterial waveforms. J Appl Physiol 2013;115 (8):1196–202.
[9] Convertino VA, Wirt MD, Glenn JF, Lein BC. The compensatory reserve for early and accurate prediction of hemodynamic compromise: a review of the underlying physiology. Shock 2016;45(6):580–90.
[10] Suresh MR. The early detection of hypovolemic shock and shifting the focus to compensation. Los Angeles, CA: SAGE Publications Sage CA; 2022.
[11] Davies SJ, Vistisen ST, Jian Z, Hatib F, Scheeren TW. Ability of an arterial waveform analysis–derived hypotension prediction index to predict future hypotensive events in surgical patients. Anesthesia Analgesia 2020;130(2):352–9.
[12] Hatib F, Jian Z, Buddi S, Lee C, Settels J, Sibert K, et al. Machine-learning algorithm to predict hypotension based on high-fidelity arterial pressure waveform analysis. Anesthesiology 2018;129(4):663–74.
[13] Dziuda Ł, Krej M, Śmietanowski M, Sobotnicki A, Sobiech M, Kwaśny P, et al. Development and evaluation of a novel system for inducing orthostatic challenge by tilt tests and lower body negative pressure. Sci Rep 2018;8(1):7793.
[14] Hansen LH, Bülow K. Feasibility of a continuous non-invasive arterial pressure (CNAP) device in a prehospital setting. Resuscitation 2014;85:S88–9.
[15] Scully CG, Selvaraj N, Romberg FW, Wardhan R, Ryan J, Florian JP, et al. Using time-frequency analysis of the photoplethysmographic waveform to detect the withdrawal of 900 mL of blood. Anesthesia Analgesia 2012;115(1):74–81.
[16] Selvaraj N, Scully CG, Shelley KH, Silverman DG, Chon KH. Early detection of spontaneous blood loss using amplitude modulation of photoplethysmogram. 2011 Annual International Conference of the IEEE Engineering in Medicine and Biology Society. IEEE; 2011. p. 5499–502.
[17] Liang Y, Chen Z, Ward R, Elgendi M. Hypertension assessment via ECG and PPG signals: An evaluation using MIMIC database. Diagnostics 2018;8(3):65.
[18] Mukkamala R, Hahn JO, Inan OT, Mestha LK, Kim CS, Töreyin H, et al. Toward ubiquitous blood pressure monitoring via pulse transit time: theory and practice. IEEE Trans Biomed Eng 2015;62(8):1879–901.
[19] Djupedal H, Nøstdahl T, Hisdal J, Landsverk SA, Høiseth LØ. Effects of experimental hypovolemia and pain on pre-ejection period and pulse transit time in healthy volunteers. Physiol Rep 2022;10(12):e15355.
[20] Elgendi M, Liang Y, Ward R. Toward generating more diagnostic features from photoplethysmogram waveforms. Diseases 2018;6(1):20.
[21] Chen Y, Yoon JH, Pinsky MR, Ma T, Clermont G. Development of hemorrhage identification model using non-invasive vital signs. Physiol Measur 2020;41(5):055010.
[22] Pinsky MR, Wertz A, Clermont G, Dubrawski A. Parsimony of hemodynamic monitoring data sufficient for the detection of hemorrhage. Anesthesia Analgesia 2020;130(5):1176.
[23] Elgendi M, Norton I, Brearley M, Abbott D, Schuurmans D. Systolic peak detection in acceleration photoplethysmograms measured from emergency responders in tropical conditions. PloS One 2013;8(10):e76585.

[24] Elgendi M, Norton I, Brearley M, Abbott D, Schuurmans D. Detection of a and b waves in the acceleration photoplethysmogram. Biomed Eng Online 2014;13(1):1–18.
[25] Elgendi M. Optimal signal quality index for photoplethysmogram signals. Bioengineering 2016;3(4):21.
[26] Mejía-Mejía E, Budidha K, Kyriacou PA, Mamouei M. Comparison of pulse rate variability and morphological features of photoplethysmograms in estimation of blood pressure. Biomed Signal Process Control 2022;78:103968.
[27] Pybus DA. Real-time, spectral analysis of the arterial pressure waveform using a wirelessly-connected, tablet computer: a pilot study. J Clin Monitor Comput 2019;33(1):53–63.
[28] Goswami N, Blaber AP, Hinghofer-Szalkay H, Convertino VA. Lower body negative pressure: physiological effects, applications, and implementation. Physiol Rev 2019;99 (1):807–51.
[29] Goswami N. Compensatory hemodynamic changes in response to central hypovolemia in humans: lower body negative pressure: updates and perspectives. J Muscle Res Cell Motility 2022:1–6.
[30] Park FS, Kay VL, Sprick JD, Rosenberg AJ, Anderson GK, Mallet RT, et al. Hemorrhage simulated by lower body negative pressure provokes an oxidative stress response in healthy young adults. Exp Biol Med 2019;244(3):272–8.
[31] Fagoni N, Bruseghini P, Adami A, Capelli C, Lador F, Moia C, et al. Effect of lower body negative pressure on phase I cardiovascular responses at exercise onset. Int J Sports Med 2020;41(04):209–18.
[32] Neumann S, Burchell AE, Rodrigues JC, Lawton CB, Burden D, Underhill M, et al. Cerebral blood flow response to simulated hypovolemia in essential hypertension: a magnetic resonance imaging study. Hypertension 2019;74(6):1391–8.
[33] Cai M, Wang H, Kline G, Ding Y, Ross SE, Davis S, et al. Habitual physical activity improves vagal cardiac modulation and carotid baroreflex function in elderly women. Exp Biol Med 2023. 15353702231160334.
[34] Wang L, Li Z, Tan C, Wang H, Zhou X, He S, et al. Lower-body negative pressure/ergometer exercise in bed rest: Effects on female orthostatic tolerance. J Novel Physiother Rehabili 2020;4(2):040–8.
[35] Jain M, Chitturi V, Chandran DS, Jaryal AK, Deepak K. Vasoconstriction during non-hypotensive hypovolemia is not associated with activation of baroreflex: A causality-based approach. Pflügers Archiv-European. J Physiol 2023:1–9.
[36] Jonsson H, Henricson J, Saager RB, Wilhelms D. Microcirculatory response to lower body negative pressure and the association to large vessel function. In: Photonics in Dermatology and Plastic Surgery 2023. vol. 12352. SPIE; 2023. p. 49–53.
[37] Harris KM, Petersen LG, Weber T. Reviving lower body negative pressure as a countermeasure to prevent pathological vascular and ocular changes in microgravity. npj Microgravity 2020;6(1):38.
[38] Van Akin M, Lantz O, Fellows A, Toutain-Kidd C, Zegans M, Buckey JC, et al. Acute effects of postural changes and lower body positive and negative pressure on the eye. Front Physiol 2022:1685.
[39] Gallardo P, Giannakopoulos I, Romare M, Karanika P, Elcadi G, et al. The Effect of Upright Lower Body Negative Pressure on Muscle Activity and Hemodynamics during Exercise. Austin Sports Med 2023;8(1):1053.
[40] Kenny JÉS, Elfarnawany M, Yang Z, Eibl AM, Eibl JK, Kim CH, et al. A wireless ultrasound patch detects mild-to-moderate central hypovolemia during lower body negative pressure. J Trauma Acute Care Surg 2022;93(2):S35.
[41] Kenny JÉS, Barjaktarevic I, Mackenzie DC, Elfarnawany M, Yang Z, Eibl AM, et al. Carotid artery velocity time integral and corrected flow time measured by a wearable Doppler ultrasound detect stroke volume rise from simulated hemorrhage to transfusion. BMC Res Notes 2022;15(1):1–5.
[42] Kenny JÉS, Elfarnawany M, Yang Z, Myers M, Eibl AM, Eibl JK, et al. The Doppler shock index measured by a wearable ultrasound patch accurately detects moderate-to-severe central hypovolemia during lower body negative pressure. J Am College Emergency Physic Open 2021;2(4):e12533.
[43] Raj KV, Nabeel P, Chandran D, Sivaprakasam M, Joseph J. High-frame-rate A-mode ultrasound for calibration-free cuffless carotid pressure: feasibility study using lower body negative pressure intervention. Blood Pressure 2022;31 (1):19–30.
[44] Kimball JP, Inan OT, Convertino VA, Cardin S, Sawka MN. Wearable Sensors and Machine Learning for Hypovolemia Problems in Occupational, Military and Sports Medicine: Physiological Basis, Hardware and Algorithms. Sensors 2022;22(2):442.
[45] Berboth L, Zirngast B, Manninger M, Steendijk P, Tschöpe C, Scherr D, et al. Graded lower body negative pressure induces intraventricular negative pressures and incremental diastolic suction: a pressure-volume study in a porcine model. J Appl Physiol 2022;133(1):20–6.
[46] Rosenberg AJ, Kay VL, Anderson GK, Sprick JD, Rickards CA. A comparison of protocols for simulating hemorrhage in humans: step versus ramp lower body negative pressure. J Appl Physiol 2021;130(2):380–9.
[47] Techentin RW, Felton CL, Schlotman TE, Gilbert BK, Joyner MJ, Curry TB, et al. 1D Convolutional neural networks for estimation of compensatory reserve from blood pressure waveforms. 2019 41st Annual International Conference of the IEEE Engineering in Medicine and Biology Society (EMBC). IEEE; 2019. p. 2169–73.
[48] Killick R, Fearnhead P, Eckley IA. Optimal detection of changepoints with a linear computational cost. J Am Stat Assoc 2012;107(500):1590–8.
[49] Ji SY. Computer-aided Trauma Decision Making Using Machine Learning and Signal Processing. 2008.
[50] Nesaragi N, Sharma A, Patidar S, Majumder S, Tavakolian K. Application of recurrent neural network for the prediction of target non-apneic arousal regions in physiological signals. In: 2018 Computing in Cardiology Conference (CinC). vol. 45; 2018. p. 1–4.
[51] Elola A, Aramendi E, Oliveira J, Renna F, Coimbra MT, Reyna MA, et al. Beyond Heart Murmur Detection: Automatic Murmur Grading from Phonocardiogram. arXiv; 2022. Available from: https://arxiv.org/abs/2209.13385.
[52] Pham TD. Time–frequency time–space LSTM for robust classification of physiological signals. Sci Rep 2021;11(1):6936.
[53] Buttkus B. Spectral analysis and filter theory in applied geophysics. Springer Science & Business Media; 2012.
[54] Salvi M, Acharya UR, Molinari F, Meiburger KM. The impact of pre-and post-image processing techniques on deep learning frameworks: A comprehensive review for digital pathology image analysis. Comput Biol Med 2021;128:104129.
[55] Shaffer F, Ginsberg JP. An overview of heart rate variability metrics and norms. Front Public Health 2017;258.
[56] Flood MW, Grimm B. EntropyHub: An open-source toolkit for entropic time series analysis. Plos One 2021;16(11):e0259448.
[57] Li T, Zhou M. ECG classification using wavelet packet entropy and random forests. Entropy 2016;18(8):285.
[58] Miao F, Fu N, Zhang YT, Ding XR, Hong X, He Q, et al. A novel continuous blood pressure estimation approach based on data mining techniques. IEEE J Biomed Health Informat 2017;21(6):1730–40.
[59] Miao F, Liu ZD, Liu JK, Wen B, He QY, Li Y. Multi-sensor fusion approach for cuff-less blood pressure measurement. IEEE J Biomed Health Informat 2019;24(1):79–91.

[60] van der Ster BJ, Westerhof BE, Stok WJ, van Lieshout JJ. Detecting central hypovolemia in simulated hypovolemic shock by automated feature extraction with principal component analysis. Physiol Rep 2018;6(22):e13895.
[61] Fadil R, Verma AK, Sadeghian F, Blaber AP, Tavakolian K. Cardio-respiratory interactions in response to lower-body negative pressure. Physiol Measur 2023;44(2):025005.
[62] Kugener G, Zhu Y, Pangal DJ, Sinha A, Markarian N, Roshannai A, et al. Deep neural networks can accurately detect blood loss and hemorrhage control task success from video. Neurosurgery 2022;90(6):823–9.
[63] Gupta JF, Arshad SH, Telfer BA, Snider EJ, Convertino VA. Noninvasive monitoring of simulated hemorrhage and whole blood resuscitation. Biosensors 2022;12(12):1168.
[64] Bedolla CN, Gonzalez JM, Vega SJ, Convertino VA, Snider EJ. An explainable machine-learning model for compensatory reserve measurement: methods for feature selection and the effects of subject variability. Bioengineering 2023;10(5):612.
[65] Chalumuri YR, Kimball JP, Mousavi A, Zia JS, Rolfes C, Parreira JD, et al. Classification of blood volume decompensation state via machine learning analysis of multi-modal wearable-compatible physiological signals. Sensors 2022;22(4):1336.
[66] Finnegan E, Davidson S, Harford M, Watkinson P, Tarassenko L, Villarroel M. Features from the photoplethysmogram and the electrocardiogram for estimating changes in blood pressure. Sci Rep 2023;13(1):986.
[67] Eid AM, Elgamal M, Gonzalez-Fiol A, Shelley KH, Wu HT, Alian AA. Using the ear photoplethysmographic waveform as an early indicator of central hypovolemia in healthy volunteers utilizing LBNP induced hypovolemia model. Physiol Meas 2023.
[68] Alian A, Shelley K, Wu HT. Amplitude and phase measurements from harmonic analysis may lead to new physiologic insights: lower body negative pressure photoplethysmographic waveforms as an example. J Clin Monitor Comput 2023;37(1):127–37.